Imaging the small animal cardiovascular system in real-time with Multispectral Optoacoustic Tomography

Adrian Taruttis[a], Eva Herzog[a], Daniel Razansky[a], Vasilis Ntziachristos[a]
[a]Institute for Biological and Medical Imaging, Helmholtz Zentrum Munich and Technical University Munich, Ingolstädter Landstraße 1, 85764 Neuherberg, Germany

ABSTRACT

Multispectral Optoacoustic Tomography (MSOT) is an emerging technique for high resolution macroscopic imaging with optical and molecular contrast. We present cardiovascular imaging results from a multi-element real-time MSOT system recently developed for studies on small animals. Anatomical features relevant to cardiovascular disease, such as the carotid arteries, the aorta and the heart, are imaged in mice. The system's fast acquisition time, in tens of microseconds, allows images free of motion artifacts from heartbeat and respiration. Additionally, we present in-vivo detection of optical imaging agents, gold nanorods, at high spatial and temporal resolution, paving the way for molecular imaging applications.

Keywords: optoacoustic tomography, photoacoustic imaging, small animal imaging, optical imaging, molecular imaging

1. INTRODUCTION

Optoacoustic (photoacoustic) imaging is emerging as a powerful technique for resolving tissue absorbers at the high spatial resolution provided by ultrasound detection[1, 2]. The method is based on the detection of ultrasonound waves generated by thermoelastic expansion of tissues arising from transient temperature increases due to the absorption of short light pulses. The amplitude of the ultrasound waves depends on the local light fluence and optical absorption properties of the tissue. Since scattering of ultrasonic waves in tissue is weak compared to scattering of light, optoacoustic imaging is able to combine the valuable contrast obtained from optical absorption with the high resolution of ultrasonic detection.

Optoacoustic imaging has a natural sensitivity to hemoglobin, the latter being the dominant absorber of light in tissues. In consequence, optoacoustic imaging has been employed to visualize vascularization, which is relevant to the understanding of tissue physiology or angiogenesis responses[1, 3-7]. While intravital optical microscopy can typically visualize vascularization with superior resolution (1–10 μm, depending on the technique) to optoacoustics (15 μm with optical resolution photacoustic microscopy[8]), the definitive advantage of optoacoustic imaging is its ability to visualize much deeper in tissues (> 1 cm) compared to the penetration limits of, for example, multi-photon microscopy (0.4–1 mm) or optical coherence tomography (< 2 mm)[9].

Using the spectral differentiation capabilities of multispectral optoacoustic tomography (MSOT), the determination of oxygenation states of hemoglobin has been demonstrated[10, 11]. Detection of atherosclerotic plaque composition based on intrinsic tissue absorption has additionally been suggested using an intravascular optoacoustic catheter system[12]. Crucially, MSOT has shown the ability to resolve molecular agents, such as fluorochromes[13, 14], fluorescent proteins[15], and other chromophoric agents[16-19] in tissues.

In this work we investigated the ability of optoacoustic imaging to resolve structures in mice that are commonly involved with cardiovascular disease (CVD), namely the carotid arteries, the aorta and the myocardium. Comparable approaches in small animal optoacoustic imaging have, for example, shown unidentified structures in a microscopic field of view in the heart region[7], macroscopic imaging of the rat thorax (post mortem) with an acquisition time of over 10 minutes[20], 3D imaging of the abdominal aorta in mice with an acquisition time of several minutes[21], or real-time imaging limited by geometry to visualizing the top of the brain[22]. We utilized a novel MSOT system that was designed for functional and molecular studies of tissue. The scanner is ideally suited for studying CVD features in mouse models as allows live imaging of physiological responses while its multispectral capability enables imaging of various exogenous optical agents with distinct spectral features. Correspondingly, we demonstrate herein imaging capabilities yielding high

Photons Plus Ultrasound: Imaging and Sensing 2011, edited by Alexander A. Oraevsky, Lihong V. Wang,
Proc. of SPIE Vol. 7899, 789913 · © 2011 SPIE · CCC code: 1605-7422/11/$18 · doi: 10.1117/12.874242

resolution transverse slices with identifiable CVD related structures and real-time visualization of gold nanorod circulation in blood vessels of the neck. In the following we describe the methods utilized, showcase the most pertinent results of the study and discuss limitations and the outlook of the technology in CVD research and clinical translation.

2. MATERIAL AND METHODS

2.1 Real-time MSOT experimental setup for in-vivo imaging

Fig. 1 shows the experimental setup used in this paper[23, 24]. It consists of a tunable optical parametric oscillator (OPO) pumped by an Nd:YAG laser (Opotek Inc., Carlsbad, CA) with a near-infrared (700-900nm) tuning range. The laser pulse duration is below 10ns and the pulse repetition frequency is 10Hz, defining the frame-rate. The beam is coupled into a fiber bundle that is divided into 10 arms on the output side which illuminate the animal from multiple angles on the imaging plane. The custom fiber bundle assembly (CeramOptic Industries, Inc., East Longmeadow, MA) consists of approximately 630 fibers, each with a fused silica core of 179 μm diameter and a numerical aperture of 0.37. The input end of the fiber bundle is fused in silica and has an active diameter of 5 mm. The fibers are then divided into 10 identical arms, each having an active diameter of 1.74 mm at the output. The assembly has a total length of approximately 2 m and has been measured to have an overall efficiency of approximately 80 % in the wavelength range from 700-850nm. The illumination on the skin surface is kept below the maximum permissible exposure (MPE) limits[24]. A custom-made piezocomposite ultrasonic transducer array (Imasonic SAS, Voray, France) with 64 elements having a central frequency of 5MHz and a bandwidth (-6dB) of 57% is used for detection. The elements are arranged in one row forming a spherical concave array covering 172° with a mechanical focal distance of 4cm. As a whole, these dimensions allow the transducer array to be considered as being cylindrically focused on the imaged plane. The time-resolved signals are digitized by an acquisition system consisting of an 18 slot PXI chassis (NI PXI-1045, National Instruments Corp., Austin, TX) containing 8 digitizer boards (NI PXI-5105, National Instruments Corp.) with 8 channels each, giving a total of 64 channels. The signals are acquired at 60MSps and 12 bit digital resolution. An embedded controller (NI PXI-8106, National Instruments Corp.) in the same chassis is used for coordinating the instrumentation via a LabVIEW (National Instruments Corp.) interface. The acquisition system is capable of acquiring data at the 10 frames-per-second limit imposed by the laser repetition rate. The transducer array and fiber bundle outputs are submerged in a water bath. Mice are placed in a prone position in a holder with a thin polyethylene membrane so that there is no direct contact between water and the mouse. This holder is positioned in the water bath so that the mouse is centered at the focal point of the transducer array. The laser beams and ultrasonic transducer array are in fixed position for all data acquisitions, whereas the animal being imaged can be translated through the imaging plane using a linear stage (NRT 150/M, Thorlabs GmbH, Dachau, Germany) to enable imaging of multiple transverse slices.

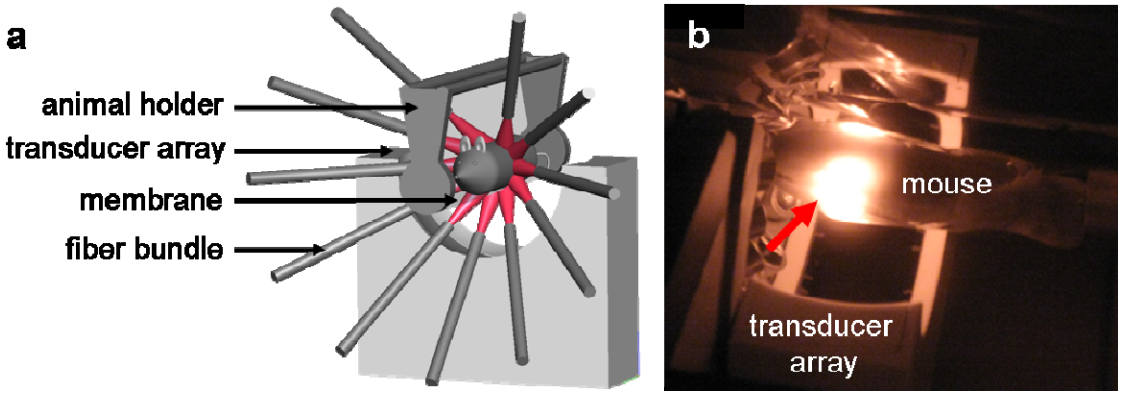

Figure 1. a: Schematic of the experimental setup. b: The setup during measurement of a mouse, where the red arrow indicates the illumination path from a fiber bundle output to the mouse.

2.2 Optical contrast agents

Commercially available gold nanorods (AuNR) with an absorption peak in the near-infrared (Ntracker 30-PM-780, Nanopartz Inc., Loveland, CO) were used to demonstrate our ability to detect exogenous contrast agents. The AuNR have, according to the manufacturer, an absorption peak around 780nm, and a per particle width of 10nm and length of 38nm.

2.3 Animal handling and imaging

Procedures involving animals and their care were conducted in conformity with the authors' institutional guidelines complying with national and international laws and regulations. Experimental protocols were reviewed and approved by the Bavarian Animal Research Authority. Adult mice (CD-1® and CD-1® Nude, Charles River Laboratories, Sulzfeld, Germany) imaged in vivo were anesthetized using ketamine/xylazine and shaved (if necessary) prior to imaging in the experimental MSOT setup and placed on the polyethylene membrane in the system in a prone position such that the transducer array faced the ventral side of the animals. For real-time operation, each two-dimensional optoacoustic image obtained utilized raw data corresponding to a single laser pulse. Mice were linearly translated in front of the detector in order to image different positions at the neck and thorax. For gold nanorod measurements, mice were scanned at 5 excitation wavelengths (725nm, 750nm, 775nm, 800nm, 825nm) using 10 signal averages per slice to serve as a control prior to agent injection. Following these reference measurements, 200µl of AuNR at a concentration of 13nM (of the nanorods themselves) were intravenously injected via the tail vein, in order to evaluate the possibility of real-time dynamic imaging of an exogenous agent. During agent injection, data from a slice through the neck were continuously acquired over 110s at 780nm. Following the dynamic measurement, the same slice was again scanned at 5 excitation wavelengths (same as above) using 10 signal averages in order to investigate the ability to spectrally differentiate the particles from background signals. Directly after imaging the mice were euthanized and frozen. For anatomical validation of the optoacoustic images, color photographs were taken during sectioning in a cryostat (CM 1950, Leica Microsystems, Wetzlar, Germany).

2.4 Image reconstruction

The images shown in this paper were reconstructed using a linear model-based inversion[25], or using a filtered backprojection algorithm[26]. In the case of the model-based inversion, once the model matrix corresponding to the fixed measurement geometry had been generated, it took approximately 14 seconds to produce a 240x240 pixel image on a PC (Intel 3 GHz Core 2 Duo with 6 GB of RAM) using Matlab software (The Mathworks Inc, Natick, MA). Images displayed in real-time on the measurement system were reconstructed using the backprojection algorithm, which took under 100ms to produce a lower resolution image. In addition, linear spectral unmixing was applied for detection of AuNR[15]. For each pixel in the image, the method fits the measured optoacoustic spectrum, normalized for variations in laser energy per wavelength, to the known absorption spectra of oxy and deoxy-hemoglobin and that of the AuNR. The fitting is performed by least-squares on the set of 5 linear equations, corresponding to the 5 measured wavelengths, generated for the 4 fitted spectra (3 known chromophore spectra and 1 constant spectrum).

3. RESULTS

3.1 Imaging of CVD relevant arteries

Fig. 2 shows optoacoustic images of the upper thorax and neck (750nm excitation). The images reveal clear signals from the aortic arch and the carotid arteries captured in transverse slices. In particular, Fig. 2a shows a slice through the top of the aortic arch and Fig. 2b shows a slice approximately 2mm above the aortic arch, revealing the innominate artery and the left common carotid artery. Fig. 2c shows the carotid arteries near the point of bifurcation, a frequent location for atherosclerotic plaque formation[27], approximately 10mm in the cranial direction from the top of the aortic arch. Here the carotid arteries are at a depth of approximately 5mm from the skin surface. Figs. 2d-f show color photographs of cryosections at corresponding locations, confirming the anatomical structures seen in the optoacoustic images. The images generally show contrast from blood vessels apart from the arteries mentioned, for example the superior vena cava.

The carotid arteries in mice have a small diameter on the order of hundreds of micrometers and are shielded by absorbing structures, such as the large veins of the neck, thus presenting a challenging imaging target. Nevertheless, as evident in

the images, the real-time optoacoustic scanner described herein, equipped with multi-angle illumination and detection, resolves these structures with sufficient contrast and resolution.

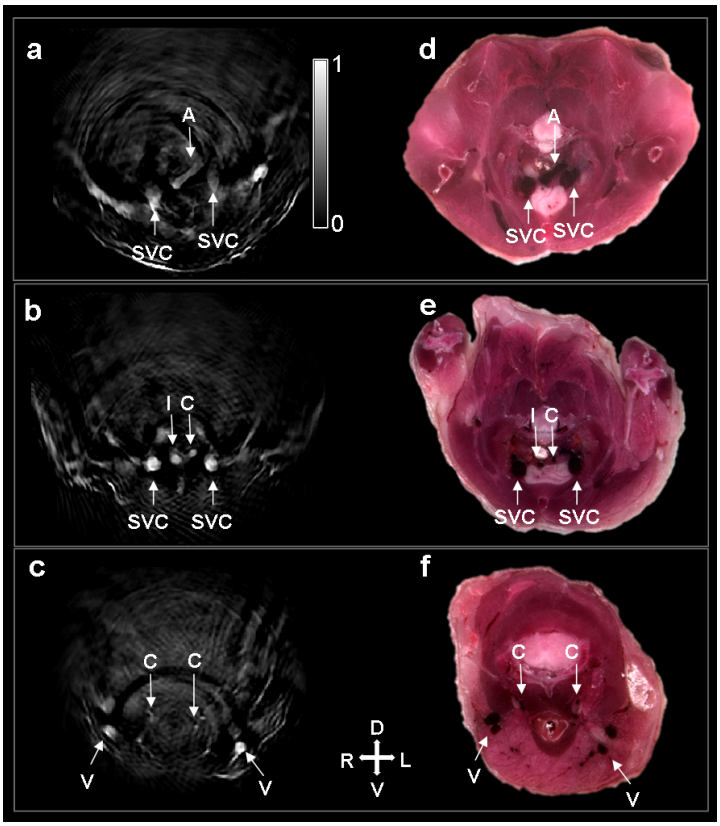

Figure 2. Transverse optoacoustic slices of arteries in the upper thorax and neck. a: Slice though top of aortic arch. A-Aortic arch. SVC-Left and right superior vena cava. b: Slice showing arteries just above aortic arch. I-Innominate artery, C-left common carotid artery, SVC-left and right superior vena cava. c: Slice approximately 10mm cranially from aortic arch showing carotid arteries near bifurcation. C-Carotid arteries, V-veins branching from external jugular vein. d-f: Photographs of cryosections showing corresponding anatomical structures to the images in a-c respectively.

3.2 Cardiac imaging

To investigate whether cardiac tissues are also visible in a noninvasive manner by optoacoustics, we performed imaging at the heart level. Fig. 3a and 3b show *in vivo* images of the anterior heart wall generated from single laser pulses (740nm) at different points in the cardiac cycle. The depth of the heart (approximately 2mm) and thickness of the heart wall (approximately 0.8mm) agree with expected values in our experience. Internal structures of the ventricles or the posterior heart wall are not clearly visible. This is likely due to the angled illumination utilized in this approach that is not optimal for imaging of the heart, where the noncylindrical shape of the mouse means that the laser beams do not all illuminate the skin surface in the imaged plane. The high attenuation of light in the blood-filled ventricles may also be a limiting factor. Since the ventricles empty of blood in every systole, it would be in principle possible to trigger the method appropriately to reduce this attenuation. Another limiting factor is the current inability of the inversion models used to account for acoustic reflections in the heart-lung interfaces and other artifacts produced by the lungs.

The information shown in the optoacoustic images in Fig. 3a and 3b is acquired within the time that it takes for the optoacoustically-generated signals to propagate from the animal toward the detectors, i.e. on the order of 50μs. This

results in images free of motion artifacts and the possibility of resolving the motion of the heart itself. Since the repetition frequency of the measurement setup is not equal to that of the heartbeat, the images captured show the heart in various stages of the cardiac cycle. In cases where a multispectral approach is used, for example to resolve exogenous contrast agents, signals from multiple pulses must be used to average out the motion per wavelength, at least in the absence of a relevant heartbeat triggering method. In this case, there is some motion-blur in the image from the heartbeat and breathing, but as shown in Fig. 3c, where images from 41 single-pulse frames are averaged, the image quality is still good enough for the heart wall to be distinguished to some extent from surrounding tissue. In Fig. 3d, the image has been averaged from 22 manually selected frames, discarding those showing ventricular systole. This selection further improves image quality by reducing motion artifacts, and can conceivably be automated using standard image processing techniques.

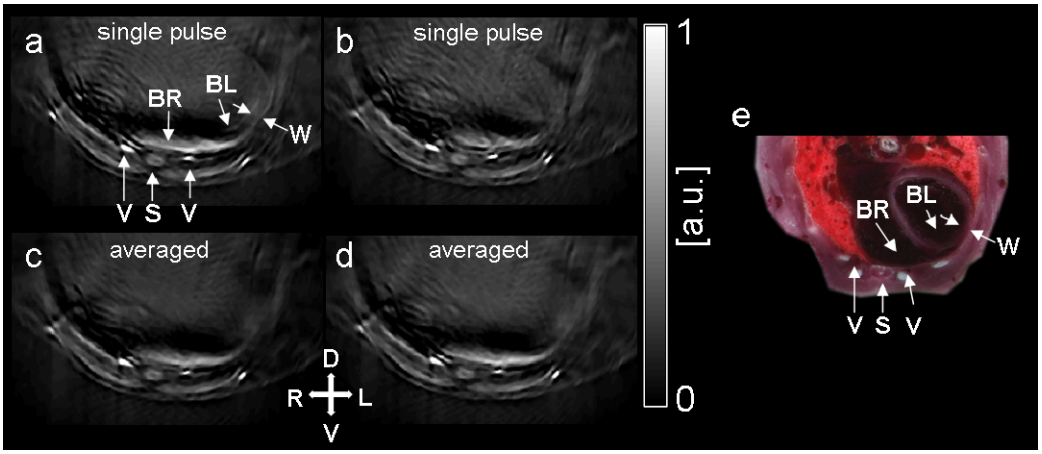

Figure 3. Optoacoustic heart imaging (740 nm excitation). a: Single-pulse image showing heart wall (W). Also visible are signals from blood inside the left and right ventricles (BL and BR) and the sternum (S) and veins (V). b: Single-pulse image taken during ventricular systole. c: Average image over 41 pulses showing motion-blur. d: Average image over 22 selected frames showing reduced motion-blur. e: Photograph of cryosection through the heart of a mouse showing features corresponding to optoacoustic images.

3.3 MSOT imaging of circulating optical agents

Fig. 4 summarizes results from imaging of AuNR, which examine the ability of the system to detect exogenous optical agents. Fig. 4a and 4b show single-pulse images (no signal averaging) from a series of acquisitions at the nominal peak absorption wavelength of the AuNR, 780 nm, made before (Fig. 4a) and after (Fig. 4b) the intravenous administration of the agent. As observed in the images, the amplitude of the signal collected from the blood vessels imaged, in particular the external jugular veins at the front of the neck, increases after AuNR injection. Because of the high absorption of light in these large blood vessels, the signal from the front of the vessels, where the excitation light is not yet attenuated, dominates the images. As observed, AuNR is detectable while circulating in the blood vessels.

Fig. 4d demonstrates MSOT imaging of AuNR aimed at investigating whether detection is possible based on its spectral profile at single timepoints. This is in contrast to the detection of AuNR based on signal differences it imparts on background measurements after administration in a time-wise fashion as described above. The image shows an MSOT result from the mouse neck after injection. Here, the multispectrally resolved signal from AuNR is overlaid on a single wavelength image (775nm) showing the relevant anatomical features. As can be seen from the images, MSOT resolves the circulating nanorods in the blood vessels. The spatial location of the resolved AuNR signal corresponds well to the

regions of increased contrast in the real-time imaging during injection. This result highlights the ability of MSOT to resolve exogenous agents *in vivo* at high resolution without need for a baseline measurement, based on their distinct spectral profile over the background tissue absorption spectrum.

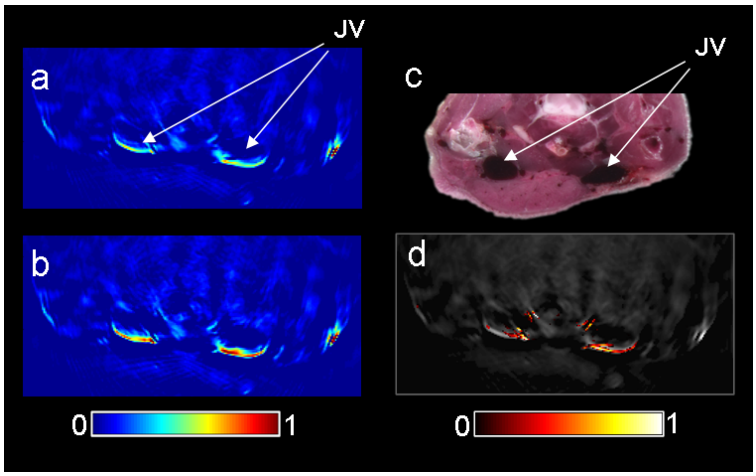

Figure 4. Optoacoustic detection of AuNR. JV-Jugular veins. a: Single-pulse transverse slice through neck prior to injection. c: The same slice 10 s after finishing the injection of AuNR. c: Photograph of cryosection showing anatomical correspondences. d: MSOT image after injection showing the multispectrally resolved distribution of AuNR overlaid on a single wavelength image.

4. DISCUSSION AND CONCLUSIONS

We have demonstrated in this paper an optoacoustic platform to image several relevant aspects of the cardiovascular system macroscopically and noninvasively in mice, including the heart, the aorta and the carotid arteries, *in vivo* and in real-time. The ability of optoacoustic imaging to resolve these structures, which play a major role in the study of cardiovascular disease, enables promising applications of the technique in biomedical discovery. In connection to this we have shown detection of gold nanorods as an exogenous optical imaging agent with a view to combining, in the future, the multispectral visualization of similar agents with the intrinsic anatomical imaging capabilities of optoacoustics to provide powerful molecular cardiovascular imaging. Real-time optoacoustic monitoring of cardiovascular dynamics in the microscopic domain has been reported on mice showing absorbers at a high frame rate[7]. However, to our knowledge, there is no other optoacoustic system reported capable of noninvasive macroscopic imaging of the small animal cardiovascular system in real-time. Our results show the heart in detail, able to clearly distinguish the anterior heart wall from blood inside the chambers. We have demonstrated dynamic imaging, free of motion artifacts from the heatbeat or respiration, which can be applied for assessing cardiac function. For multispectral imaging of the heart, where motion between different wavelengths requires, in the absence of synchronization or triggering methods, averaging of multiple signals, we have shown that anatomical structures can still be recognized. Manual selection of images at similar points in the cardiac cycle improves averaged image quality.

In addition to the possibility to extract morphological information from the images, exogenous contrast agents highlighting biological targets would provide a method for molecular imaging of the cardiovascular system. Here, we have been able to detect gold nanorods circulating in the bloodstream, both by dynamic imaging of the resulting contrast enhancement at a single wavelength close to the absorption peak of the agent, and by use of the MSOT technique to resolve the unique spectral signature of the agent *in vivo*. Gold nanorods show high absorption (molar extinction coefficient on the order of 10^8 $M^{-1}cm^{-1}$) with absorption peaks tunable by adjusting their aspect ratios, making them especially suitable for use in MSOT imaging. The resolving power of MSOT combined with gold nanorods demonstrated in our imaging platform indicates the feasibility of cardiovascular molecular imaging using gold nanorods conjugated to targeting ligands, promising such applications as visualization of infarct healing, inflammation in

atherosclerotic plaques, tracking of stem cell therapy and many others[28]. Furthermore, the macroscopic imaging demonstrated here on mice indicates that it may be possible to apply these methods to clinical diagnosis of CVD, for example, on relevant targets such as the carotid arteries in the human neck.

REFERENCES

[1] R. A. Kruger, W. L. Kiser, D. R. Reinecke et al., "Thermoacoustic molecular imaging of small animals," Molecular imaging: official journal of the Society for Molecular Imaging, 2(2), 113 (2003).

[2] M. Xu, and L. V. Wang, "Photoacoustic imaging in biomedicine," Review of Scientific Instruments, 77, 041101 (2006).

[3] S. Manohar, S. E. Vaartjes, J. C. G. van Hespen et al., "Initial results of in vivo non-invasive cancer imaging in the human breast using near-infrared photoacoustics," Optics Express, 15(19), 12277-12285 (2007).

[4] K. Maslov, G. Stoica, and L. V. Wang, "In vivo dark-field reflection-mode photoacoustic microscopy," Optics letters, 30(6), 625-627 (2005).

[5] J. J. Niederhauser, M. Jaeger, R. Lemor et al., "Combined ultrasound and optoacoustic system for real-time high-contrast vascular imaging in vivo," IEEE transactions on medical imaging, 24(4), 436-440 (2005).

[6] X. Wang, Y. Pang, G. Ku et al., "Noninvasive laser-induced photoacoustic tomography for structural and functional in vivo imaging of the brain," Nature Biotechnology, 21(7), 803-806 (2003).

[7] R. J. Zemp, L. Song, R. Bitton et al., "Realtime photoacoustic microscopy of murine cardiovascular dynamics," Optics express, 16(22), 18551-18556 (2008).

[8] K. Maslov, H. F. Zhang, S. Hu et al., "Optical-resolution photoacoustic microscopy for in vivo imaging of single capillaries," Optics Letters, 33(9), 929-931 (2008).

[9] F. Kiessling, D. Razansky, and F. Alves, "Anatomical and microstructural imaging of angiogenesis," European Journal of Nuclear Medicine and Molecular Imaging, (Epub ahead of print) (2010).

[10] J. Laufer, D. Delpy, C. Elwell et al., "Quantitative spatially resolved measurement of tissue chromophore concentrations," Physics in medicine and biology, 52, 141-168 (2007).

[11] H. F. Zhang, K. Maslov, M. Sivaramakrishnan et al., "Imaging of hemoglobin oxygen saturation variations in single vessels in vivo using photoacoustic microscopy," Applied Physics Letters, 90, 053901 (2007).

[12] S. Sethuraman, J. H. Amirian, S. H. Litovsky et al., "Spectroscopic intravascular photoacoustic imaging to differentiate atherosclerotic plaques," Optics Express, 16(5), 3362-3367 (2008).

[13] M. L. Li, J. T. Oh, X. Xie et al., "Simultaneous molecular and hypoxia imaging of brain tumors in vivo using spectroscopic photoacoustic tomography," Proceedings of the IEEE, 96(3), 481-489 (2008).

[14] D. Razansky, C. Vinegoni, and V. Ntziachristos, "Multispectral photoacoustic imaging of fluorochromes in small animals," Optics Letters, 32(19), 2891-2893 (2007).

[15] D. Razansky, M. Distel, C. Vinegoni et al., "Multispectral opto-acoustic tomography of deep-seated fluorescent proteins in vivo," Nature Photonics, 3(7), 412-417 (2009).

[16] A. De La Zerda, C. Zavaleta, S. Keren et al., "Carbon nanotubes as photoacoustic molecular imaging agents in living mice," Nature nanotechnology, 3(9), 557-562 (2008).

[17] M. Eghtedari, A. Oraevsky, J. A. Copland et al., "High sensitivity of in vivo detection of gold nanorods using a laser optoacoustic imaging system," Nano Letters, 7(7), 1914-1918 (2007).

[18] P. C. Li, C. R. C. Wang, D. B. Shieh et al., "In vivo photoacoustic molecular imaging with simultaneous multiple selective targeting using antibody-conjugated gold nanorods," Optics Express, 16(23), 18605-18615 (2008).

[19] V. Ntziachristos, and D. Razansky, "Molecular Imaging by Means of Multispectral Optoacoustic Tomography (MSOT)," Chem. Rev, 110(5), 2783-2794 (2010).

[20] K. H. Song, and L. V. Wang, "Noninvasive photoacoustic imaging of the thoracic cavity and the kidney in small and large animals," Medical physics, 35, 4524 (2008).

[21] H. P. Brecht, R. Su, M. Fronheiser et al., "Whole-body three-dimensional optoacoustic tomography system for small animals," Journal of Biomedical Optics, 14, 064007 (2009).

[22] J. Gamelin, A. Maurudis, A. Aguirre et al., "A real-time photoacoustic tomography system for small animals," Optics express, 17(13), 10489-10498 (2009).
[23] A. Buehler, E. Herzog, D. Razansky et al., "Video rate optoacoustic tomography of mouse kidney perfusion," Opt. Lett., 35(14), 2475-2477 (2010).
[24] A. Taruttis, E. Herzog, D. Razansky et al., "Real-time imaging of cardiovascular dynamics and circulating gold nanorods with multispectral optoacoustic tomography," Optics Express, 18(19), 19592-19602 (2010).
[25] A. Rosenthal, D. Razansky, and V. Ntziachristos, "Fast semi-analytical model-based acoustic inversion for quantitative optoacoustic tomography," Medical Imaging, IEEE Transactions on, 29(6), 1275 - 1285 (2010).
[26] R. A. Kruger, D. R. Reinecke, and G. A. Kruger, "Thermoacoustic computed tomography–technical considerations," Medical Physics, 26, 1832 (1999).
[27] C. K. Zarins, D. P. Giddens, B. K. Bharadvaj et al., "Carotid bifurcation atherosclerosis. Quantitative correlation of plaque localization with flow velocity profiles and wall shear stress," Circulation Research, 53(4), 502 (1983).
[28] F. A. Jaffer, P. Libby, and R. Weissleder, "Molecular imaging of cardiovascular disease," Circulation, 116(9), 1052 (2007).